

Article

Enhanced Stomatal Conductance Supports Photosynthesis in Wheat to Improved NH_4^+ Tolerance

Jinling Hu [†], Qiaomei Zheng [†], Chaofeng Dong, Zihui Liang, Zhongwei Tian and Tingbo Dai ^{*}

Key Laboratory of Crop Physiology Ecology and Production Management of Ministry of Agriculture, Nanjing Agricultural University, Nanjing 210095, China; 2018201007@njau.edu.cn (J.H.); 2020201015@stu.njau.edu.cn (Q.Z.); 2021101015@stu.njau.edu.cn (C.D.); 2015101019@njau.edu.cn (Z.L.); zhwitian@njau.edu.cn (Z.T.)

^{*} Correspondence: tingbod@njau.edu.cn; Tel.: +86-025-84395033

[†] These authors contributed equally to this work.

Abstract: The impact of ammonium (NH_4^+) stress on plant growth varies across species and cultivars, necessitating an in-depth exploration of the underlying response mechanisms. This study delves into elucidating the photosynthetic responses and differences in tolerance to NH_4^+ stress by investigating the effects on two wheat (*Triticum aestivum* L.) cultivars, Xumai25 (NH_4^+ -less sensitive) and Yangmai20 (NH_4^+ -sensitive). The cultivars were grown under hydroponic conditions with either sole ammonium nitrogen (NH_4^+ , AN) or nitrate nitrogen (NO_3^- , NN) as the nitrogen source. NH_4^+ stress exerted a profound inhibitory effect on seedling growth and photosynthesis in wheat. However, these effects were less pronounced in Xumai25 than in Yangmai20. Dynamic photosynthetic analysis revealed that the suppression in photosynthesis was primarily attributed to stomatal limitation associated with a decrease in leaf water status and osmotic potential. Compared to Yangmai20, Xumai25 exhibited a significantly higher leaf K^+ concentration and *TaAKT1* upregulation, leading to a stronger stomatal opening and, consequently, a better photosynthetic performance under NH_4^+ stress. In conclusion, our study suggested stomatal limitation as the primary factor restricting photosynthesis under NH_4^+ stress. Furthermore, we demonstrated that improved regulation of osmotic substances contributed to higher stomatal conductance and enhanced photosynthetic performance in Xumai25.

Keywords: ammonium stress; photosynthesis; wheat; stomatal conductance; osmotic potential



Citation: Hu, J.; Zheng, Q.; Dong, C.; Liang, Z.; Tian, Z.; Dai, T. Enhanced Stomatal Conductance Supports Photosynthesis in Wheat to Improved NH_4^+ Tolerance. *Plants* **2024**, *13*, 86. <https://doi.org/10.3390/plants13010086>

Academic Editor: Fermin Morales

Received: 19 November 2023

Revised: 22 December 2023

Accepted: 25 December 2023

Published: 27 December 2023



Copyright: © 2023 by the authors. Licensee MDPI, Basel, Switzerland. This article is an open access article distributed under the terms and conditions of the Creative Commons Attribution (CC BY) license (<https://creativecommons.org/licenses/by/4.0/>).

1. Introduction

It is well known that ammonium (NH_4^+), though a principal nitrogen source, can induce plant toxicity, particularly when used as the sole or predominant nitrogen source [1–3]. Several studies have investigated the manifestations of NH_4^+ stress in plants, including diminished biomass, elevated reactive oxygen species (ROS) production, disruptions in pH equilibrium, and ion regulation [2,4]. The sensitivity of plants to NH_4^+ stress is inherently variable, contingent upon factors such as species, genotypes, and soil conditions [1,4,5]. Though NH_4^+ assimilation heavily relies on the sugar generated during photosynthesis in the leaves, extant research has predominantly concentrated on the mechanisms underlying NH_4^+ uptake and assimilation in plant roots [6,7]. A discernible knowledge gap exists in how NH_4^+ stress affects photosynthesis, especially in susceptible plant species.

During photosynthesis, the diffusion of CO_2 from the atmosphere to the chloroplast sites for carboxylation encounters multiple resistances within leaves. The regulatory mechanism underlying stomatal opening is well elucidated [8]. It comprises an initial influx of K^+ , which is later replaced by sucrose, culminating in a reduction of sucrose levels [9]. Recent investigations in rice plants have demonstrated that K^+ deficiency can reduce stomatal conductance, restricting gas exchange [10]. Furthermore, NH_4^+ absorption has been shown to impede the uptake of other cations, such as K^+ or Ca^{2+} , and elevate

ABA content [4,11]. Thus, NH_4^+ stress might instigate a reduction in stomatal conductance, adversely impacting photosynthesis.

While the regulation of stomatal conductance (g_s) and transpiration by nitrogen nutrition is a well-established tenet in plant physiology, the impact of excess NH_4^+ on transpiration and water use efficiency (WUE) remains unclear. Intriguingly, distinct nitrogen forms can impart divergent effects on plant water uptake, this phenomenon is intricately linked to the nitrogen preference of various plant species [12]. Some studies posit that excessive NH_4^+ can inhibit plant water uptake [13] or induce symptoms akin to water deficit, termed “ammoniacal syndrome” [14]. Conversely, other studies argue that compared to NO_3^- nutrition, NH_4^+ nutrition can further strengthen water stress resistance in rice via marked upregulation of AQP genes [12,15]. Thus, the influence of NH_4^+ stress on the water status of plants and its intricate relationship to stomatal opening and subsequent photosynthetic capacity remain unclear.

Chlorophyll fluorescence, closely linked to chlorophyll content, emerges as a crucial indicator of the photosynthetic response to stress [16]. NH_4^+ stress adversely impacts the chlorophyll content of plants, however, the degree of impact depends on the severity of stress and the plant species [17,18]. Previous studies have postulated that NH_4^+ stress can disrupt the stability of leaf membrane lipids, hindering electron transfer and consequently impeding photosynthesis [19]. In contrast, a previous study in *Arabidopsis* showed that NH_4^+ stress elevates mitochondrial ROS levels without significant impacts on photosynthesis [20]. Such divergent findings warrant the need to comprehensively elucidate the regulatory mechanisms governing chlorophyll content and chlorophyll fluorescence under NH_4^+ stress.

Wheat, a key part of global food production, is well known for its high susceptibility to NH_4^+ toxicity [21,22]. In wheat seedlings, NH_4^+ stress is manifested as stunted seedling growth and the onset of oxidative stress [21]. The pivotal role of nitrogen in the metabolism of photosynthetic pigments and the efficient functioning of the photosynthetic apparatus underscores its profound impact on overall plant growth and development, including in wheat. Despite the indispensable role of nitrogen in photosynthesis, the specific photosynthetic response of wheat seedlings to NH_4^+ stress remains unknown. The primary objective of this study was to delve into the mechanism underlying the tolerance and photosynthetic response of wheat seedlings to NH_4^+ stress. Here, we conducted a comparative analysis of two wheat cultivars: NH_4^+ -less sensitive Xumai25 and NH_4^+ -sensitive Yangmai20. We focused on growth responses, gas exchange, leaf water status, and adjustments in osmotic balance in both these cultivars in response to NH_4^+ stress.

2. Results

2.1. Plant Growth and Nitrogen Concentration

The impact of NH_4^+ stress (AN) on plant growth was evident from the significantly lower dry weight of AN-treated plants than NN-treated plants at 10 DAT, with a more pronounced decrease in Yangmai20 (25%) than Xumai25 (7%). Similarly, the AN-treated plants exhibited reduced leaf area, with a more pronounced reduction in Yangmai20 than Xumai25 (Table 1). In contrast, the AN-treated plants showed higher specific leaf weight (SLW) and nitrogen concentration than the NN-treated plants, with a more pronounced increase in Yangmai20.

2.2. Photosynthesis and Related Attributes

The AN-treated plants exhibited a progressive decline in the net photosynthetic rate (A) (Figure 1A) from 1 to 10 DAT, with a more pronounced decline observed in NH_4^+ -sensitive Yangmai20. At 5 DAT, the value of A was significantly reduced in Yangmai20 under NH_4^+ stress compared to NN-treated plants, but this phenomenon was not observed in Xumai25. Furthermore, AN significantly reduced stomatal conductance (g_s), sub-stomatal CO_2 concentration (C_i), and transpiration rate (Tr) in Yangmai20 (Figure 1B,D,E), compared to the NN (17%, 11%, and 13%, respectively). In contrast, AN substantially increased

stomatal limitation (l) in both cultivars, with consistently higher stomatal limitation, evidenced by lower g_s , in Yangmai20 than in Xumai25 (Figure 1B,F). Additionally, AN did not significantly affect leaf mesophyll conductance (g_m) (Figure 1C), carboxylation efficiency (CE), electron transfer rate (J_e), maximum carboxylation rate (V_{max}), or maximum electron transport rate (J_{max}) in either cultivar (Figure 2A–D).

Table 1. Effects of ammonium stress on dry weight, leaf area, leaf nitrogen concentration, and specific leaf weight of wheat seedling at 10 days after treatment.

Cultivar	Treatment	Plant Dry Weight (mg plant ⁻¹)	Plant Leaf Area (cm ² plant ⁻¹)	Leaf Nitrogen Concentration (mg g ⁻¹)	Specific Leaf Weight of 4th Leaf (mg cm ⁻² DW)
Yangmai20	NN	1266 ± 39.7 a	100 ± 4.6 a	69 ± 1.9 b	0.30 ± 0.008 b
	AN	980 ± 31.2 c	82 ± 5.4 c	77 ± 2.5 a	0.38 ± 0.017 a
Xumai25	NN	1128 ± 50.3 b	97 ± 4.7 ab	65 ± 3.1 b	0.29 ± 0.013 b
	AN	1033 ± 50.2 c	86 ± 3.4 bc	75 ± 2.2 a	0.37 ± 0.006 a

Note: NN, nitrate treatment; AN, ammonium treatment. Data are means ± standard deviation (SD) of three biological replicates, and different letters indicate significant differences ($p < 0.05$) according to ANOVA.

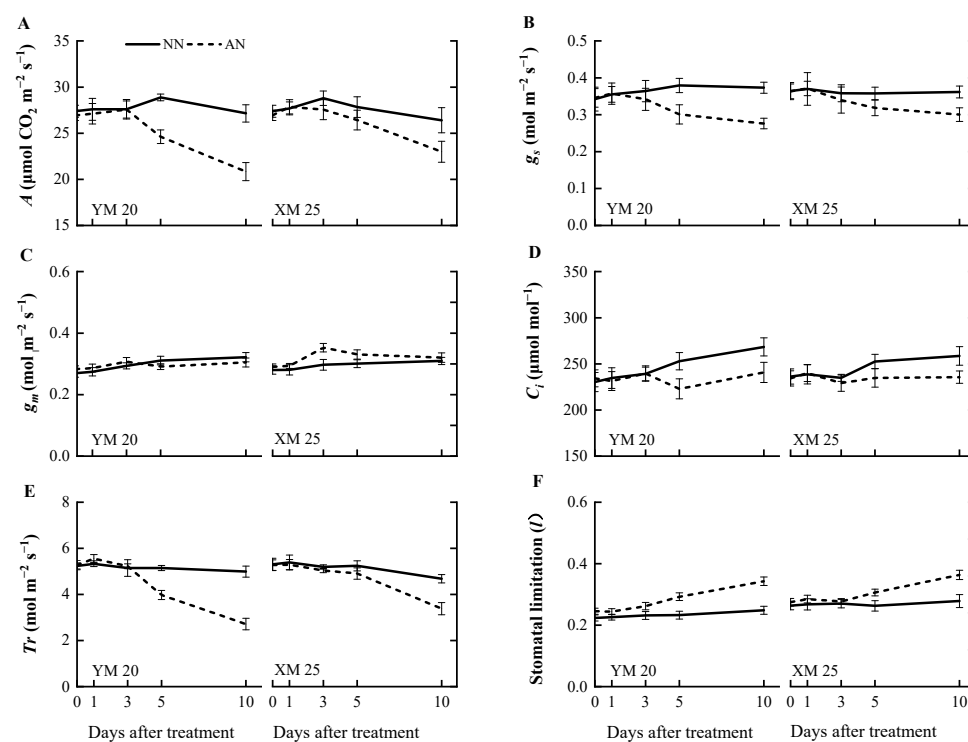


Figure 1. Effects of ammonium stress on (A) net photosynthetic rate (A), (B) stomatal conductance (g_s), (C) leaf mesophyll conductance (g_m), (D) sub-stomatal CO₂ concentration (C_i), (E) transpiration rate (Tr), and (F) stomatal limitation (l) of wheat seedlings at 0, 1, 3, 5, and 10 days after treatment. NN, nitrate treatment; AN, ammonium treatment. YM20, Yangmai20 (NH₄⁺-sensitive); XM25, Xumai25 (NH₄⁺-less sensitive).

Furthermore, at 10 DAT, AN led to a significant decline in CE , V_{max} , and J_e of Yangmai20 but did not markedly impact the corresponding parameters in Xumai25 (Figure 2A–C).

2.3. Chlorophyll Content and Chlorophyll Fluorescence Parameters

Changes in chlorophyll content and chlorophyll fluorescence were concurrently measured alongside photosynthetic parameters. The AN-treated Yangmai20 exhibited slightly elevated total chlorophyll content at 3 and 5 DAT, while this phenomenon was not observed in Xumai25. However, there was no significant difference in the total chlorophyll content of the AN- and NN-treated plants at 10 DAT (Figure 3A). Notably, no significant

differences were observed in the actual photochemical efficiency ($Y(II)$) of AN- and NN-treated Xumai25 (Figure 3B–D). In contrast, the $Y(II)$ value of AN-treated Yangmai20 was significantly lower than NN-treated Yangmai20 at 10 DAT (Figure 3B). Furthermore, no significant differences were observed in the maximum quantum yield (Fv/Fm) of the AN- and NN-treated plants. The non-photochemical quenching (NPQ) of AN-treated plants was significantly higher than NN-treated plants at 10 DAT.

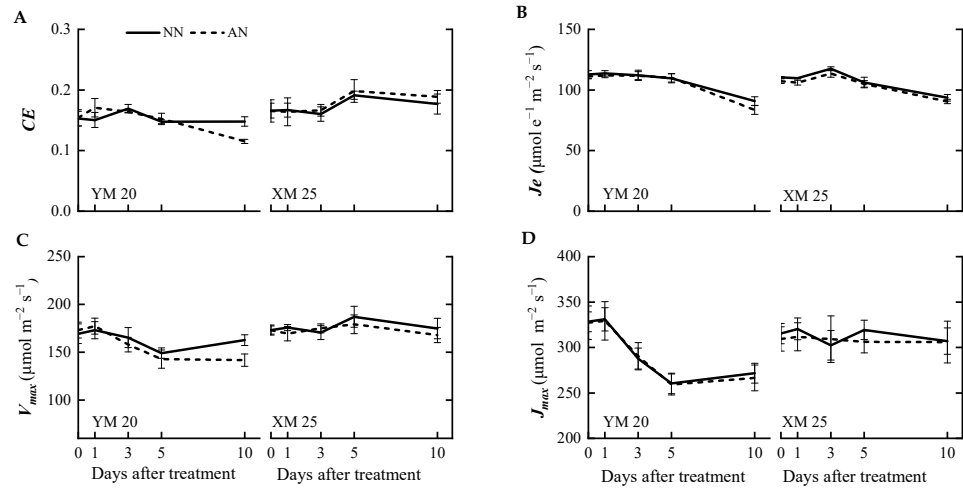


Figure 2. Effects of ammonium stress on the (A) carboxylation efficiency (CE), (B) electron transfer rate (J_e), (C) maximum carboxylation rate (V_{max}), and (D) the maximum electron transport rate (J_{max}), at 0, 1, 3, 5, and 10 days after treatment NN, nitrate treatment; AN, ammonium treatment. YM20, Yangmai20 (NH_4^+ -sensitive); XM25, Xumai25 (NH_4^+ -less sensitive).

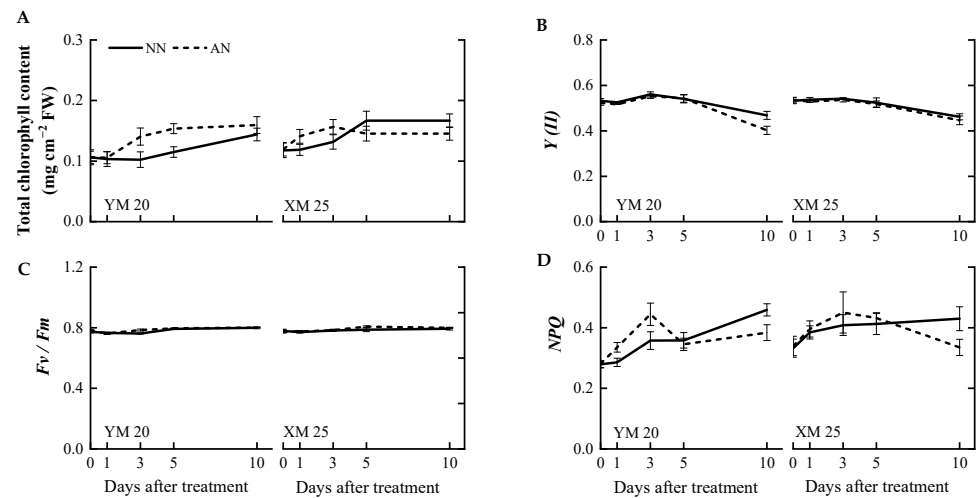


Figure 3. Effects of ammonium stress on (A) total chlorophyll content, (B) actual photochemical efficiency ($Y(II)$), (C) maximum quantum yield (Fv/Fm), and (D) non-photochemical quenching (NPQ) of wheat seedlings at 0, 1, 3, 5, and 10 days after treatment. NN, nitrate treatment; AN, ammonium treatment. YM20, Yangmai20 (NH_4^+ -sensitive); XM25, Xumai25 (NH_4^+ -less sensitive).

2.4. Leaf Moisture Status

AN treatment adversely impacted the leaf moisture status compared to the NN treatment. At 5 DAT, AN-treated Yangmai20 exhibited significantly reduced relative water content (RWC), pre-dawn water potential (ψ_p), osmotic potential (ψ_s), and midday water potential (ψ_m) compared to NN-treated Yangmai20, while no significant differences were observed between AN- and NN-treated Xumai25. At 10 DAT, the AN-treated plants exhibited a decrease in RWC, ψ_s , ψ_p , and ψ_m , with a more pronounced decrease in Yangmai20 (Figure 4A–D).

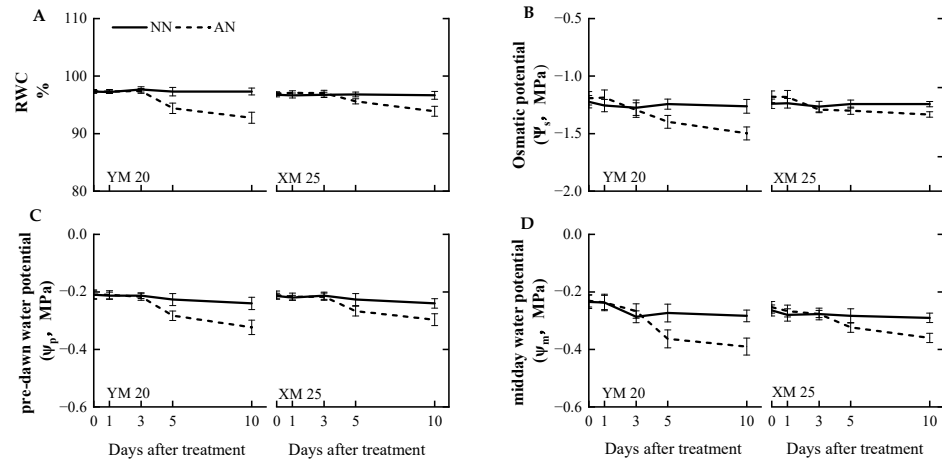


Figure 4. Effects of ammonium stress on the (A) relative water content (RWC), (B) leaf osmotic potential (ψ_s), (C) pre-dawn water potential (ψ_p), and (D) midday water potential (ψ_m) of wheat seedlings at 0, 1, 3, 5, and 10 days after treatment (DAT). NN, nitrate treatment; AN, ammonium treatment. YM20, Yangmai20 (NH₄⁺-sensitive); XM25, Xumai25 (NH₄⁺-less sensitive).

2.5. Concentration of K⁺, Sucrose and ABA

AN treatment significantly impacted the parameters related to osmotic homeostasis and stomatal opening. All AN-treated plants exhibited consistently decreasing K⁺ and sucrose levels (Figure 5A,B). Although, Xumai25 exhibited substantially less pronounced K⁺ reduction than Yangmai20 (Figure 5A). In addition, AN-treated Yangmai20 exhibited higher ABA concentration in the leaves than NN-treated plants at 5 DAT, while no significant differences were observed between AN- and NN-treated Xumai25. At 10 DAT, ABA concentration was significantly increased in both cultivars under AN treatment (Figure 5C).

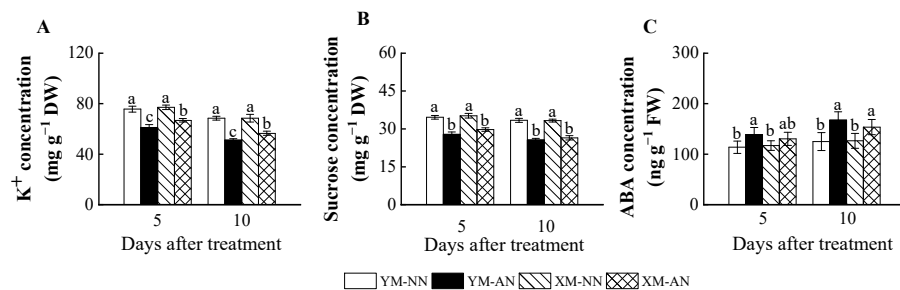


Figure 5. Effects of ammonium stress on (A) K⁺, (B) sucrose, and (C) ABA concentration of wheat seedlings at 5 and 10 days after treatment. Different letters indicate significant differences ($p < 0.05$) according to ANOVA. NN, nitrate treatment; AN, ammonium treatment. YM, Yangmai20 (NH₄⁺-sensitive); XM, Xumai25 (NH₄⁺-less sensitive).

2.6. Relative Gene Expression

In leaves, the AN-treated plants exhibited higher *TaHA1* and *TaAKT1* expression than NN-treated plants in both cultivars (Figure 6A,B). Furthermore, AN-treated Yangmai20 exhibited significantly lower *TaKOR1* expression than NN-treated Yangmai20, while no significant difference was observed between AN- and NN-treated Xumai25 (Figure 6C). However, the *TaKAT1* expressions of AN- and NN-treated Yangmai20 were comparable to AN- and NN-treated Xumai25, respectively (Figure 6D).

In roots, AN-treated Yangmai20 exhibited significantly lower *TaTIP2.3* and *TaPIP1.1* expression than NN-treated Yangmai20, while this phenomenon is not observed in Xumai25 (Figure 6E,F). Moreover, the AN-treated plants exhibited higher *TaAKT1* expression than NN-treated plants, with significantly higher expression in AN-treated Xumai25 than NN-treated Xumai25 (Figure 6G).

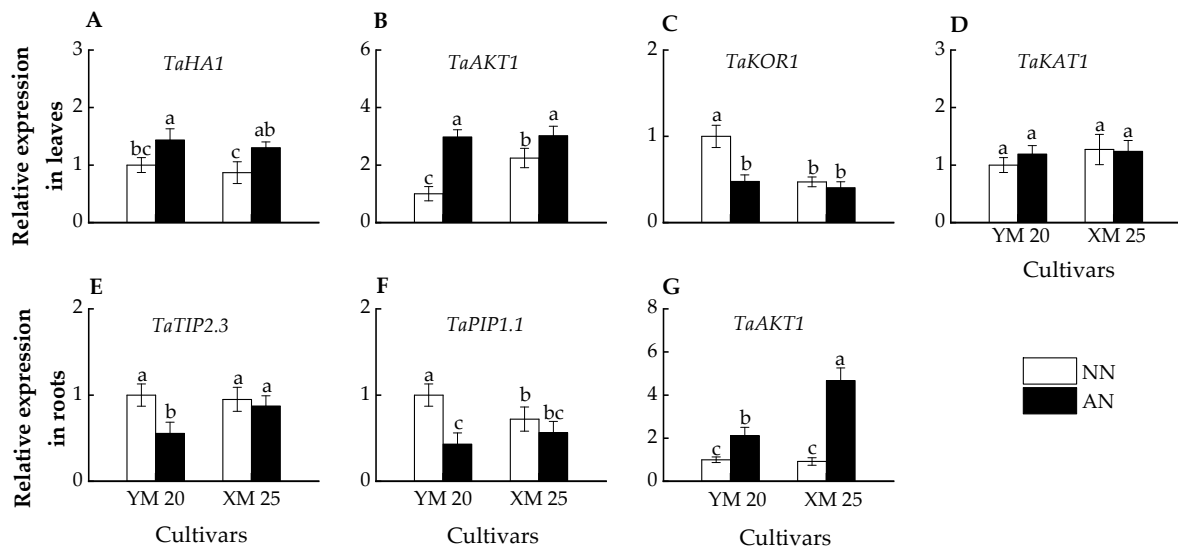


Figure 6. Effects of ammonium stress on the expressions of genes encoding K^+ channel, water channel, and proton transport protein in leaves and roots of wheat seedlings at 5 days after treatment, including (A) *TaHA1*, (B) *TaAKT1*, (C) *TaKOR1*, (D) *TaKAT1*, (E) *TaTIP2.3*, (F) *TaPIP1.1*, (G) *TaAKT1*. Data are expressed as means of three biological replicates, and different letters indicate significant differences ($p < 0.05$) according to ANOVA. NN, nitrate treatment; AN, ammonium treatment. YM, Yangmai20 (NH_4^+ -sensitive); XM, Xumai25 (NH_4^+ -less sensitive).

2.7. The Relationships between Photosynthetic Parameters and Physiological Traits with Nitrogen Forms

Principal component analysis (PCA) demonstrated that PC1 and PC2 explained 74.3% of the total trait variance for the two wheat cultivars under the two treatments (AN and NN) (Figure 7). The eigenvalue and cumulative contribution of PC1 and PC2 of photosynthetic parameter and physiological traits and their corresponding loading are shown in Supplementary Table S1. PC1 explained 56.8% of total variation and had a positive association with ψ_m , ψ_s , ψ_p , K^+ , g_s , and A , and a negative association with l . Thus, PC1 tended to represent traits like leaf moisture status, osmotic substance, and photosynthetic parameters. Alternatively, PC2 explained 17.5% of the total variation and was positively associated with NPQ and $Y(II)$, representing the chlorophyll fluorescence. These results indicated that photosynthetic traits might be positively related to leaf moisture status and osmotic substance, and were negatively correlated to l .

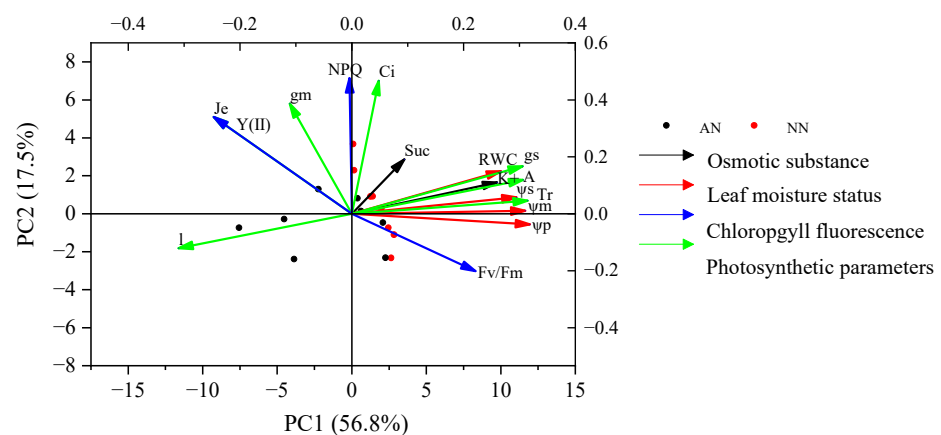


Figure 7. Cont.

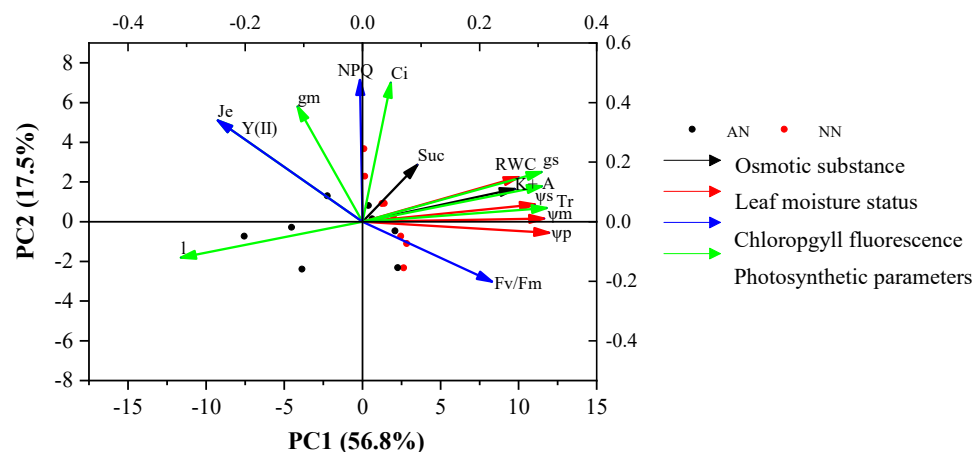


Figure 7. Principal component analysis (PCA) of photosynthetic parameters and other physiological traits of two wheat cultivars (Yangmai20 and Xumai25) under AN and NN treatments. NN, nitrate treatment; AN, ammonium treatment.

3. Discussion

Diverse plant species and cultivars manifest distinctive responses to NH_4^+ stress, as demonstrated by studies on peas [23], tomatoes [24], and *Arabidopsis* [25]. Several studies have extensively reported the NH_4^+ sensitivity of wheat [21,26]. In this study, the deleterious impact of NH_4^+ stress on the biomass and photosynthesis of wheat seedlings (Table 1 and Figure 1A) is similar to the effects reported in other plant species [2,27]. Notably, upon NH_4^+ stress, the NH_4^+ -less sensitive cultivar Xumai25 demonstrated a mitigated reduction in net photosynthetic rate (A) compared to the NH_4^+ -sensitive cultivar Yangmai20, resulting in superior dry matter production (Table 1, Figure 1A).

3.1. Variation in Photosynthetic Response and Stomatal Limitation

Photosynthesis, intricately linked to NH_4^+ tolerance [28], involves limitation and biochemical limitations influencing photosynthetic capacity. Our findings indicated that Yangmai20 exhibited a notable reduction in A , g_s , C_i , and an increase in l (Figure 1A–D). However, parameters related to the photosynthetic dark reaction, such as CE , J_e , V_{max} , and J_{max} , did not differ significantly between AN- and NN-treated plants (Figure 2A–D). Previous studies have demonstrated l to be a critical factor in reducing A when both C_i and g_s decrease [29,30]. Thus, in the present study, l might predominantly contribute to the reduced photosynthesis in wheat under NH_4^+ stress. Consistent with our findings, NH_4^+ stress has previously been found to induce stomatal closure in tomatoes [28], and reduction in rice [31] and wheat [32]. Notably, Xumai25 exhibited a less pronounced decrease in g_s at 5 DAT, indicating its superior ability to maintain the open state of stomata, contributing to enhanced photosynthetic performance under NH_4^+ stress. Furthermore, at 10 DAT, the dark reaction parameters (CE , V_{max} , and J_e) significantly decreased in Yangmai20 under prolonged NH_4^+ stress (Figure 2A,C,D), illustrating a delayed response, which might be attributed to initial CO_2 assimilation induced by reduced g_s [33].

3.2. Leaf Mesophyll Conductance (g_m) under NH_4^+ Stress

The impact of NH_4^+ on g_m varies based on the plant species and severity of the stress. For instance, Liu et al. (2021) [34] found a significantly lower g_m in female *Populus cathayana* plants after being supplied with NH_4^+ under salt stress than after being supplied with NO_3^- . In contrast, Li et al. (2012) [35] reported a significantly higher g_m in NH_4^+ -supplied rice than NO_3^- -supplied rice under drought stress. In the present study, however, we did not observe a significant difference in g_m between AN- and NN-treated plants (Figure 1C). The observed variations in g_m can be attributed to two factors. First, increased NH_4^+ assimilation products augmented the specific leaf weight (SLW) in both

cultivars (Table 1), influencing CO₂ partial pressure inside chloroplasts, which can increase g_m [36]. Second, heightened leaf nitrogen content (Table 1) after NH₄⁺ stress possibly led to increased cell wall thickness [37].

3.3. Chlorophyll Concentration and Fluorescence under NH₄⁺ Stress

The impact of NH₄⁺ stress on chlorophyll content varies based on stress severity, plant species, and cultivars [18]. For instance, several studies have reported a decrease in the chlorophyll content of *Arabidopsis* in the presence of high NH₄⁺ levels [17,38]. In contrast, some studies have reported increased and decreased chlorophyll content after mild and severe NH₄⁺ stress, respectively [18]. In the present study, the chlorophyll content in both cultivars was not markedly different between NN-treated and AN-treated plants (Figure 3A), suggesting that 5 mM NH₄⁺ was considered a moderate stress level for wheat seedlings. Additionally, chlorophyll content is closely associated with the efficiency of electron transport and photosynthesis. For instance, Chen et al. (2023) [27] demonstrated that NH₄⁺ exposure disrupts the electron transport chain in citrus plants. Interestingly, in this study, we did not observe any significant difference in J_e as A decreased in Yangmai20 at 5 DAT and in Xumai25 at 10 DAT. Chlorophyll fluorescence measurements indicated no significant damage to the PSII reaction centers during the treatment period, as evident by the unchanged Fv/Fm in both cultivars (Figure 3C). The reduction in $Y(II)$ in AN-treated Yangmai20 (Figure 3B) might be responsible for the decrease in J_e (Figure 2B). In addition, the increase in NPQ in AN-treated plants was possibly related to photorespiration [39].

3.4. Decline in Stomatal Conductance and Osmotic Potential under NH₄⁺ Stress

Several factors, such as stomatal morphology, distribution, and movement, influence g_s , a pivotal determinant of photosynthesis [40]. The focus of the current investigation was the nuanced impact of NH₄⁺ stress on g_s , with specific attention to the intricate regulation of stomatal movement. We meticulously examined the newest fully expanded leaves before treatment initiation to circumvent potential confounding effects from stomatal morphology and distribution. Stomatal movement, primarily orchestrated by the changes in the turgor pressure and volume of the guard cells, is governed by major osmotic entities, such as K⁺ and sucrose [8]. Our findings revealed a marked reduction in the leaf osmotic potential (Ψ_s) of Yangmai20 since 5 DAT (Figure 4B), aligning with the decline in g_s . This finding indicates a direct correlation between diminishing Ψ_s under NH₄⁺ stress and the consequential reduction in stomatal aperture.

Recent research emphasizes the pivotal role of sucrose and K⁺ as primary solutes influencing the guard cell osmotic potential [8,9]. K⁺ deficiency has been shown to reduce leaf water potential and stomatal area in rice, resulting in a decline in photosynthesis [10]. In the current study, a notable reduction in leaf K⁺ concentration was observed for both wheat cultivars under NH₄⁺ stress, with a more pronounced reduction in Yangmai20 (Figure 5A). Intriguingly, our study unveiled a higher *TaAKT1* upregulation under NH₄⁺ stress in the roots of Xumai25 than Yangmai20 (Figure 6G), potentially contributing to the higher K⁺ concentration in Xumai25. Moreover, we observed a significant decrease in the sucrose level of both cultivars under NH₄⁺ stress (Figure 1A), which potentially decreases osmotic potential. The decreased sucrose concentration is potentially linked to inhibited photosynthesis (Figure 1A) and increased carbon skeleton requirements due to ammonium assimilation in the roots [2]. Taken together, the reduction in K⁺ and sucrose levels under NH₄⁺ stress led to a decrease in leaf osmotic potential, which in turn resulted in a decrease in g_s . Xumai25, benefiting from its higher leaf K⁺ concentration, sustained an elevated Ψ_s under NH₄⁺ stress, thus maintaining an enhanced g_s .

Additionally, meticulous K⁺ flux regulation in guard cells, facilitated by inward (KAT) and outward rectifying K⁺ channels (KOR), also plays a crucial role [41]. Our study revealed a significant *TaKOR1* downregulation in Yangmai20 in response to NH₄⁺ stress (Figure 6C), with no significant response in Xumai25. In contrast, no significant alteration in *TaKAT1* expression was observed in any of the cultivars (Figure 6D). This finding indicates

that the high K^+ concentration and influx in NH_4^+ -less sensitive cultivars contributed to the consistently high osmotic potential under NH_4^+ stress. Additionally, both cultivars exhibited *TaHAI1* upregulation (Figure 6A), indicating the crucial role of K^+ flow [42] in NH_4^+ stress responses. Further, ABA has been demonstrated to activate anion channels in the plasma membrane of guard cells, leading to anion efflux and subsequent release of K^+ from guard cells, resulting in stomatal closure under drought stress [42]. The elevated ABA level observed in our study (Figure 5C) further contributes to decreased g_s . However, the nuanced interplay of NH_4^+ stress with ion channels governing osmotic potential in stomatal guard cells warrants further exploration. Our results provide an initial foundation for understanding this intricate relationship.

3.5. Water Uptake under NH_4^+ Stress

In the current study, the impact of NH_4^+ exposure on water uptake in the plants remained non-definitive. Some studies suggested that NH_4^+ nutrition enhances water absorption [15,43] while some studies proposed that exposure to NH_4^+ significantly inhibits water uptake in plants [13]. The present study observed a significant reduction in RWC and ψ_m in both cultivars, with a more pronounced effect in Yangmai20 (Figure 4A,D). Moreover, NH_4^+ stress prompted a substantial downregulation of *TaTIP2.3* and *TaPIP1.1* in Yangmai20 (Figure 6E,F). These findings indicate a more pronounced impact of NH_4^+ stress on water uptake in Yangmai20 than in Xumai25. Based on the existing literature, we postulate that this phenomenon might be attributed to two factors. First, the downregulation of AQPs under NH_4^+ stress to mitigate NH_3/NH_4^+ absorption and transport, as some studies have reported that aquaporins (AQPs) can transport NH_3/NH_4^+ [12,44]. Second, the cellular acidification induced by NH_4^+ stress [2], as evidenced by *TaHAI1* upregulation (Figure 6A), adversely impacts the activity of AQPs [45].

4. Materials and Methods

4.1. Plant Materials and Experimental Design

Two wheat cultivars, Xumai25 (NH_4^+ -less sensitive) and Yangmai20 (NH_4^+ -sensitive), were subjected to hydroponic experiments. The seeds were surface-sterilized using a 10% (*v/v*) H_2O_2 solution for 15 min and subsequently rinsed thoroughly with sterile distilled water. Subsequently, the seeds were germinated under dark conditions in Petri dishes until the seed bud length reached approximately 1 cm (typically 36 h). Then, the seedlings were transplanted into water-filled opaque plastic containers (45 cm × 32 cm × 25 cm, volume 36 L). When the seedlings reached the two-leaf stage, they were transferred to a modified 50% Hoagland nutrient solution and grown until they reached the four-leaf stage. After this pre-treatment, the seedlings were divided into two groups, each group comprising seedlings from both cultivars. One group was treated with nitrate nitrogen (NN, 5 mM NO_3^- -N) nutrient solution and the other with NH_4^+ nitrogen (AN, 5 mM NH_4^+ -N) nutrient solution. The macronutrient compositions of both treatment solutions are detailed in Supplementary Table S2. The micronutrient composition was kept consistent in both treatment solutions, as described previously [21]. The solutions were refreshed every three days to ensure a consistent nitrogen supply in each solution and were continuously aerated to prevent anoxia. The pH of each solution was adjusted daily to 5.8 using either 0.1 mM H_2SO_4 or 0.1 mM NaOH. The entire experiment was conducted in a controlled greenhouse environment with a 16 h/8 h light/dark cycle and temperature maintained at 18 °C during the day and 8.5 °C at night. The light intensity and relative air humidity in the greenhouse were set at 400 $\mu\text{mol m}^{-2} \text{s}^{-1}$ and 60%, respectively. We adopted a completely randomized block design, and each experiment was replicated three times. Each replication consisted of 3 containers, and each container housed 60 plants.

The random seedlings (belonging to both cultivars) from both groups were collected at 0, 1, 3, 5, and 10 days after treatment (DAT). The fourth leaf (the newest fully expanded leaf before treatment) was used for the measurement of photosynthetic, fluorescence, and leaf water status parameters. The fourth leaves, other leaves, stems, and roots of the collected

seedlings were separated and divided into two segments. One segment was oven-dried at 105 °C for 20 min, followed by drying at 85 °C, to determine the dry weight and nitrogen concentration measurements. The other segment was promptly frozen in liquid nitrogen and stored at −80 °C for subsequent analyses.

4.2. Gas Exchange Measurements

Gas exchange measurements were constructed using a gas exchange system (Li-Cor 6800, Li-Cor Inc. Lincoln, NE, USA) equipped with a standard chamber (2 cm²) and a Multiphase Flash Fluorometer (6800-01F). The parameters were set as follows: leaf temperature, 25.0 ± 0.5 °C; steady-state photosynthetic photon flux density (PPFD), 1200 μmol photons m^{−2} s^{−1}; vapor pressure deficit (VPD), 1.1 ± 0.05 kPa; and relative humidity, 55–65%. Leaves were introduced into the chamber at a reference CO₂ concentration of 400 μmol mol^{−1} for 10 min for stabilization before measurement. Parameters including net photosynthetic rate (*A*), sub-stomatal CO₂ concentration (*C_i*), stomatal conductance (*g_s*), transpiration rate (*Tr*), and electron transport rate (*J_e*) were recorded after stabilization.

For the *A*–*C_i* curves, the reference CO₂ concentration was systematically adjusted to the following levels: 400, 200, 150, 100, 50, 400, 400, 600, 800, 1000, 1200, and 1500 μmol mol^{−1}. Data were recorded, following a stabilization period of 2–3 min at each level. Six leaves from each treatment group were selected for this experiment. Carboxylation efficiency (*CE*) was calculated as the initial slope of the *A*–*C_i* curves when *C_i* was <200 μmol mol^{−1} [46]. Parameters such as maximum carboxylation rate (*V_{max}*), RuBP regeneration (*J_{max}*), mesophyll conductance (*g_m*), and stomatal limitation (*l*) were determined using a modified equation derived from the works of S. P. Long and C. J. Bernacchi [47] and Li et al. [46].

The photosynthetic rate (*A*) was expressed mathematically as:

$$A = v_c - 0.5v_o - Rd = v_c (1 - \Gamma^*/C_i) - Rd \quad (1)$$

Here, *v_c* is the Rubisco carboxylation rate, *v_o* is the Rubisco oxygenation rate, *Rd* is the mitochondrial respiration rate in the light, and Γ^* is the CO₂ compensation point related to the *C_i* [46]. Here, *v_c* is determined by the minimum of three potential rates: potential Rubisco carboxylation rate, RuBP regeneration rate, and triose phosphate utilization (TPU) rate, (*w_c*, *w_j*, and *w_p*, respectively):

$$v_c = \min(w_c, w_j, w_p) \quad (2)$$

Also:

$$w_c = (V_{max} \times C_i) / (C_i + K_c \times (1 + O/K_o)) \quad (3)$$

$$w_j = (J_{max} \times C_i) / (4.5 C_i + 10.5 \Gamma^*) \quad (4)$$

Here, *O* is the O₂ concentration (210 mmol mol^{−1}). Furthermore,

$$K_c = \exp^{(38.05 - 79.43/(R \times (T + 273.15)))} \quad (5)$$

$$K_o = \exp^{(20.30 - 36.38/(R \times (T + 273.15)))} \quad (6)$$

Here, *K_c* and *K_o* are the Michaelis constants of carboxylation and oxygenation, respectively. *T* is the leaf temperature (°C).

The *A*–*C_i* curve comprises three phases. In the first phase, Rubisco is limiting and *J_e* increases with the increase in *C_i*. Thus Equation (3) can be fitted to Equations (1) and (2) as follows:

$$A = V_{max} \times C_i \times (1 - \Gamma^*/C_i) / (C_i + K_c \times (1 + O/K_o)) - Rd \quad (7)$$

Setting *f* as a variable changing with *C_i*:

$$f = C_i \times (1 - \Gamma^*/C_i) / (C_i + K_c \times (1 + O/K_o)) \quad (8)$$

Equation (8) can then be rewritten as follows:

$$A = V_{max} \times f - Rd \quad (9)$$

Thus, A can be plotted as a linear function of f , where V_{max} is the slope and Rd is the intercept.

In the second phase, RuBP regeneration is limiting and J_e remains constant with increasing C_i . Thus, Equation (4) can be fitted to Equations (1) and (2) as follows:

$$A = J_{max} \times C_i \times (1 - \Gamma^*/C_i)/(4.5 C_i + 10.5 \Gamma^*) - Rd \quad (10)$$

Setting g as a variable changing with C_i :

$$g = C_i \times (1 - \Gamma^*/C_i)/(4.5 C_i + 10.5 \Gamma^*) \quad (11)$$

Equation (11) can then be written as follows:

$$A = J_{max} \times g - Rd \quad (12)$$

Thus, A can be plotted as a linear function of g , where J_{max} is the slope and Rd is the intercept.

Stomatal limitation (l) was calculated as follows:

$$l = (A'' - A')/A'' \quad (13)$$

Here, A' is the net photosynthetic rate at the ambient atmospheric CO_2 concentration ($400 \mu\text{mol mol}^{-1}$) and A'' is the net photosynthetic rate when C_i is equal to ambient atmospheric CO_2 concentration ($C_i = 400 \mu\text{mol mol}^{-1}$).

The leaf mesophyll conductance (g_m) was calculated using the constant J method [47,48]:

$$g_m = A/(C_i - \Gamma^* (J_e + 8(A + Rd))/(J_e - 4(A + Rd))) \quad (14)$$

Here, J_e is the electron transport rate.

4.3. Leaf Area and Chlorophyll Fluorescence Measurements

Plant leaf areas were measured using an LI-3100 AREA METER (Li-Cor, Inc., Lincoln, NE, USA).

After the photosynthetic measurements, the fluorescence characteristics of the fourth leaves were determined using a PAM-2500 portable chlorophyll fluorescence apparatus (PAM-2500, Walz, Germany). The leaves were dark-adapted for 30 min before measurements. The minimum fluorescence, F_o , and the maximal fluorescence yield, F_m , were recorded after executing a saturation pulse. Then the actinic light ($497 \mu\text{mol photons m}^{-2} \text{s}^{-1}$) was opened, and the saturation pulses were generated. The initial fluorescence F_o' , the maximum fluorescence F_m' , and the steady fluorescence F_t were recorded during this progress. The maximum quantum yield of the PSII reaction center (F_v/F_m), the actual photochemical efficiency ($Y(II)$), and the non-photochemical quenching (NPQ) were calculated using a modified equation developed by Christof Klughammer (2008) [49]. The equation is as follows:

$$F_v/F_m = (F_m - F_o)/F_m \quad (15)$$

$$Y(II) = (F_m' - F)/F_m' \quad (16)$$

$$NPQ = F_m/F_m' - 1 \quad (17)$$

4.4. Leaf Water Status

The pre-dawn water potential (ψ_p) and midday water potential (ψ_m) of the fourth leaf were determined during the pre-dawn period (between 04:00 and 05:00) and noon (between 12:00 and 13:00), respectively, using a Model 1505D-EXP Pressure Chamber Instrument (1505D-EXP, Decagon, Albany, OR, USA). Briefly, the leaf veins were vertically cut using a sharp blade and the leaf veins were immediately placed into the pressure chamber. The

water potential was recorded as the pressure at which blisters emerged on the cross-section of the leaf.

The osmotic potential (Ψ s) of the fourth leaf was determined using a vapor pressure osmometer (Wescor 5600, Wescor Inc., Logan, UT, USA) at 25 °C. Briefly, the leaf was flash-frozen in liquid nitrogen at 9:00–10:00 a.m. Then, cell sap was extracted through maceration and filtration using fine nylon mesh and a syringe. The osmotic potential was then calculated from the instrument, as per the manufacturer's instructions.

The leaf relative water content (RWC) of the fourth leaf was measured using a previously described protocol [50]. Briefly, the leaves were weighed immediately after harvest and the weight was recorded as W_f . Then, the leaves were immersed in distilled water for 12 h and weighed to obtain the saturated fresh weight (W_t). Subsequently, the leaves were dried to a constant weight in an oven at 85 °C and weighed to obtain the dry weight (W_d). The RWC was calculated using the formula: $(W_f - W_d) / (W_t - W_d) \times 100\%$.

4.5. Determination of N, K+ and Sucrose Concentration

Fresh fourth leaves were freeze-dried and then ground into a powder.

For N and K concentration analyses, approximately 0.1 g of the sample powder was mixed with 5 mL of H_2SO_4 . The resulting mixture was heated to 200 °C until a clear solution was obtained. Subsequently, the reaction was terminated by adding H_2O_2 . The resulting solutions were then analyzed using inductively coupled plasma optical emission spectrometry (ICP-OES, Optima 8000, Perkin Elmer, Waltham, MA, USA).

The sucrose concentration was determined using the resorcinol method as described by Zeng et al. (2014) [51]. Briefly, 0.1 g of the sample powder was weighed and extracted with a sugar extraction solution. The mixture was centrifuged ($15,000 \times g$, 15 min), and the supernatant was collected. Next, 0.3 mL of the supernatant was mixed with 0.1 mL of 2 M NaOH, and the solution was incubated at 95 °C for 10 min. Next, 1 mL of 0.1 M resorcinol and 3.5 mL of 10 M HCl were added to the mixture, and the solution was incubated at 80 °C for 60 min. The OD of the solution was measured at 500 nm using UV/VIS spectrophotometer (Pharmacia, Cambridge, UK). The sucrose concentration was calculated using the standard curve.

4.6. Determination of ABA Concentration

ABA concentration was determined using the method described by Greco et al. (2012) [52], with some modifications. Briefly, approximately 0.5 g of the fresh leaf sample was weighed and added to a pre-cooled mortar with 5 mL of 50% chromatographic grade methanol (v/v) and ground into a slurry in an ice bath. The slurry was then extracted at 4 °C in the dark for 12 h. Afterward, the mixture was centrifuged at 10,000 r/min for 10 min at 4 °C, and the supernatant was collected and stored in a refrigerator. The residue from the first extraction was subjected to two more extractions. For the second extraction, 4 mL pre-cooled 80% chromatographic grade methanol was added to the residue, and the mixture was again extracted for 12 h, followed by centrifugation. The same progress was repeated for the third extraction using 2 mL of pre-cooled 100% chromatographic grade methanol. All supernatants from the three extractions were combined. To adsorb phenols and pigments, PVPP (0.2 g/g FW) was added to the supernatants, which were then shaken at 4 °C for 60 min and centrifuged as mentioned above. The resulting supernatant was slowly passed through a prepared C18 column, and the effluent was collected and freeze-dried in the dark. After freeze-drying, the sample was dissolved in 3 mL of 50% chromatographic grade methanol, filtered through a 0.22 μ m membrane, and finally injected into an ultra-performance liquid chromatography (UPLC) system (ACQUITY UPLC H-Class system, Waters, Milford, MA, USA) for analysis. The UPLC analysis was performed using an ACQUITY UPLC HSS T3 column (100 mm \times 2.1 mm \times 1.8 μ m, Waters).

4.7. RT-PCR Analysis

Total RNA was extracted from root and leaf samples using TRIzol reagent (Vazyme Bio, Nanjing, China). The HiScript III Q RT SuperMix (Vazyme Bio, Nanjing, China) was used for cDNA synthesis as per the manufacturer's instructions. The cDNA samples were then diluted 5-fold and subjected to qPCR analysis. qRT-PCR was conducted using the CFX Connect Real-Time PCR Detection System (Bio-Rad, Hercules, CA, USA) with ChamQ SYBR qPCR Master Mix (Vazyme Bio, China).

The primer sequence for *TaHa1* was sourced from Jiang et al. [53]. The primers for aquaporins (*TaTIP2.3*, and *TaPIP1.1*) were sourced from Wu et al. [54]. The primers for potassium transport channel (AKT1) were designed using Primer 5 software. The primers for potassium ion inflow channel (KAT1), and potassium ion outflow channel (KOR1) were sourced from the work of Yang et al. [55]. ACT and ADP genes were used as internal references. All primer sequence is listed in Supplementary Table S3. Relative expression levels were determined using a previously described method [56].

4.8. Statistical Analysis

Physiological data derived from both dry and fresh samples were calculated using three biological replicates, while the data pertaining to photosynthetic, fluorescence, and water status parameters of the leaves were derived from six leaf replicates. Analysis of variance (ANOVA), followed by the Tukey HSD test was used for multiple comparisons. SPSS 26 (IBM, Armonk, NY, US) was used for all statistical analyses. Graphs and tables were generated using Origin 2021 software (OriginLab, Northampton, MA, USA) and Microsoft Excel.

5. Conclusions

In conclusion, our study showed that 5 mM NH_4^+ stress significantly disrupted the crucial photosynthetic processes in wheat plants. Our findings highlight the predominant stomatal limitation in photosynthesis under NH_4^+ stress conditions. In this process, K^+ mediated Ψ_s decrease played a vital role in the decline of g_s . In addition, the NH_4^+ -less sensitive cultivar exhibited a robust ability to maintain osmotic homeostasis, resulting in higher g_s and improved photosynthetic performance and growth under NH_4^+ stress. Further studies are still needed to elucidate how high NH_4^+ concentrations might impact, at the molecular and electrophysiological levels, the stomatal opening in higher plants.

Supplementary Materials: The following supporting information can be downloaded at: <https://www.mdpi.com/article/10.3390/plants13010086/s1>. Table S1. Eigenvalue and cumulative contribution of PCs of photosynthetic parameter and their corresponding loading. Table S2. The concentration and components of macronutrients in both treatments. Table S3. The primer sequence in this study.

Author Contributions: J.H.: experimentalize, writing—original draft preparation. Q.Z.: experimentalize, data analysis. C.D.: experimentalize. Z.L.: revision. Z.T.: supervision. T.D.: methodology, supervision. All authors have read and agreed to the published version of the manuscript.

Funding: This research was funded by the National Natural Science Foundation of China (Grant No. 32272215) and the National Key R&D Program of Jiangsu (BE2021361-1).

Data Availability Statement: The data presented in this study are available on request from the corresponding author. The data are not publicly available due to we have an in-depth research project on this topic in the future.

Acknowledgments: We express our appreciation to the other researchers and staff members involved in this project for their valuable contributions, expertise, and assistance in project management.

Conflicts of Interest: The authors declare that they have no known competing financial interests or personal relationships that could have appeared to influence the work reported in this paper.

References

1. Britto, D.T.; Kronzucker, H.J. NH_4^+ toxicity in higher plants: A critical review. *J. Plant Physiol.* **2002**, *159*, 567. [CrossRef]

2. Esteban, R.; Ariz, I.; Cruz, C.; Moran, J.F. Review: Mechanisms of ammonium toxicity and the quest for tolerance. *Plant Sci.* **2016**, *248*, 92. [[CrossRef](#)] [[PubMed](#)]
3. Liu, Y.; von Wirén, N. Ammonium as a signal for physiological and morphological responses in plants. *J. Exp. Bot.* **2017**, *68*, 2581. [[CrossRef](#)] [[PubMed](#)]
4. Bittsánszky, A.; Pilinszky, K.; Gyulai, G.; Komives, T. Overcoming ammonium toxicity. *Plant Sci.* **2015**, *231*, 184. [[CrossRef](#)] [[PubMed](#)]
5. Marino, D.; Moran, J.F. Can Ammonium Stress Be Positive for Plant Performance? *Front. Plant Sci.* **2019**, *10*, 1–5. [[CrossRef](#)] [[PubMed](#)]
6. Bejarano, I.; Marino, D.; Coletto, I. Arabidopsis MYB28 and MYB29 transcription factors are involved in ammonium-mediated alterations of root-system architecture. *Plant Signal Behav.* **2021**, *16*, 1879532. [[CrossRef](#)] [[PubMed](#)]
7. Robert, G.; Yagy, M.; Koizumi, T.; Naya, L.; Masclaux Daubresse, C.; Yoshimoto, K. Ammonium stress increases microautophagic activity while impairing macroautophagic flux in Arabidopsis roots. *Plant J.* **2021**, *105*, 1083. [[CrossRef](#)]
8. Emily, L.; Harrison, L.A.C.J. The influence of stomatal morphology and distribution on photosynthetic gas exchange. *Plant J.* **2020**, *101*, 768.
9. Cochrane, T.T.; Cochrane, T.A. Differences in the way potassium chloride and sucrose solutions effect osmotic potential of significance to stomata aperture modulation. *Plant Physiol. Biochem.* **2009**, *47*, 205. [[CrossRef](#)]
10. Yang, C.; Zhang, J.; Zhang, G.; Lu, J.; Ren, T.; Cong, R.; Lu, Z.; Zhang, Y.; Liao, S.; Li, X. Potassium deficiency limits water deficit tolerance of rice by reducing leaf water potential and stomatal area. *Agric. Water Manag.* **2022**, *271*, 107744. [[CrossRef](#)]
11. Li, B.; Li, G.; Kronzucker, H.J.; Baluška, F.; Shi, W. Ammonium stress in Arabidopsis: Signaling, genetic loci, and physiological targets. *Trends Plant Sci.* **2014**, *19*, 107. [[CrossRef](#)] [[PubMed](#)]
12. Gao, L.; Lu, Z.; Ding, L.; Guo, J.; Wang, M.; Ling, N.; Guo, S.; Shen, Q. Role of Aquaporins in Determining Carbon and Nitrogen Status in Higher Plants. *Int. J. Mol. Sci.* **2018**, *19*, 35. [[CrossRef](#)] [[PubMed](#)]
13. Naku, M.; Kambizi, L.; Matimati, I. Functional roles of ammonium (NH₄⁺) and nitrate (NO₃⁻) in regulation of day- and night-time transpiration in *Phaseolus vulgaris*. *Funct. Plant Biol.* **2019**, *46*, 806. [[CrossRef](#)] [[PubMed](#)]
14. Cramer, M.D.; Hawkins, H.; Verboom, G.A. The importance of nutritional regulation of plant water flux. *Oecologia* **2009**, *161*, 15. [[CrossRef](#)] [[PubMed](#)]
15. Ding, L.; Gao, C.; Li, Y.; Li, Y.; Zhu, Y.; Xu, G.; Shen, Q.; Kaldenhoff, R.; Kai, L.; Guo, S. The enhanced drought tolerance of rice plants under ammonium is related to aquaporin (AQP). *Plant Sci.* **2015**, *234*, 14. [[CrossRef](#)] [[PubMed](#)]
16. Hu, H.; Wang, L.; Wang, Q.; Jiao, L.; Hua, W.; Zhou, Q.; Huang, X. Photosynthesis, chlorophyll fluorescence characteristics, and chlorophyll content of soybean seedlings under combined stress of bisphenol A and cadmium. *Environ. Toxicol. Chem.* **2014**, *33*, 2455. [[CrossRef](#)] [[PubMed](#)]
17. Rah, M.; Helali, S.; Nebli, H.; Kaddour, R.; Mahmoudi, H.; Lachaâl, M.; Ouerghi, Z. Influence of nitrate—Ammonium ratio on growth and nutrition of *Arabidopsis thaliana*. *Plant Soil* **2010**, *336*, 65.
18. Sanchez-Zabala, J.; Gonzalez-Murua, C.; Marino, D. Mild ammonium stress increases chlorophyll content in *Arabidopsis thaliana*. *Plant Signal Behav.* **2015**, *10*, e991596. [[CrossRef](#)]
19. Patterson, K.; Cakmak, T.; Cooper, A.; Lager, I.D.; Rasmusson, A.G.; Escobar, M.A. Distinct signalling pathways and transcriptome response signatures differentiate ammonium- and nitrate-supplied plants. *Plant Cell Environ.* **2010**, *33*, 1486–1501. [[CrossRef](#)]
20. Podgórska, A.; Gieczewska, K.; Łukawska-Kuzma, K.; Rasmusson, A.G.; Gardeström, P.; Szal, B. Long-term ammonium nutrition of Arabidopsis increases the extra chloroplastic NAD(P)H/NAD(P)⁺ ratio and mitochondrial reactive oxygen species level in leaves but does not impair photosynthetic capacity. *Plant Cell Environ.* **2013**, *36*, 2034. [[CrossRef](#)]
21. Liu, Y.; Li, Y.; Li, Y.; Tian, Z.; Hu, J.; Adkins, S.; Dai, T. Changes of oxidative metabolism in the roots of wheat (*Triticum aestivum* L.) seedlings in response to elevated ammonium concentrations. *J. Integr. Agric.* **2021**, *20*, 1216. [[CrossRef](#)]
22. Ijato, T.; Porras Murillo, R.; Ganz, P.; Ludewig, U.; Neuhäuser, B. Concentration-dependent physiological and transcriptional adaptations of wheat seedlings to ammonium. *Physiol. Plant.* **2021**, *171*, 328. [[CrossRef](#)] [[PubMed](#)]
23. Cruz, C.; Domínguez-Valdivia, M.D.; Aparicio-Tejo, P.M.; Lamsfus, C.; Bio, A.; Martins-Loução, M.A.; Moran, J.F. Intra-specific variation in pea responses to ammonium nutrition leads to different degrees of tolerance. *Environ. Exp. Bot.* **2011**, *70*, 233. [[CrossRef](#)]
24. Vega-Mas, I.; Rossi, M.T.; Gupta, K.J.; González-Murua, C.; Ratcliffe, R.G.; Estavillo, J.M.; González-Moro, M.B. Tomato roots exhibit in vivo glutamate dehydrogenase aminating capacity in response to excess ammonium supply. *J. Plant Physiol.* **2019**, *239*, 83. [[CrossRef](#)] [[PubMed](#)]
25. Hachiya, T.; Inaba, J.; Wakazaki, M.; Sato, M.; Toyooka, K.; Miyagi, A.; Kawai-Yamada, M.; Sugiura, D.; Nakagawa, T.; Kiba, T.; et al. Excessive ammonium assimilation by plastidic glutamine synthetase causes ammonium toxicity in *Arabidopsis thaliana*. *Nat. Commun.* **2021**, *12*, 4944. [[CrossRef](#)] [[PubMed](#)]
26. Vega-Mas, I.; Cukier, C.; Coletto, I.; González-Murua, C.; Limami, A.M.; González-Moro, M.B.; Marino, D. Isotopic labelling reveals the efficient adaptation of wheat root TCA cycle flux modes to match carbon demand under ammonium nutrition. *Sci. Rep.* **2019**, *9*, 8925. [[CrossRef](#)]
27. Chen, H.; Hu, W.; Wang, Y.; Zhang, P.; Zhou, Y.; Yang, L.; Li, Y.; Chen, L.; Guo, J. Declined photosynthetic nitrogen use efficiency under ammonium nutrition is related to photosynthetic electron transport chain disruption in citrus plants. *Sci. Hortic.* **2023**, *308*, 111594. [[CrossRef](#)]

28. Vega-Mas, I.; Marino, D.; Sánchez-Zabala, J.; González-Murua, C.; Estavillo, J.M.; González-Moro, M.B. CO₂ enrichment modulates ammonium nutrition in tomato adjusting carbon and nitrogen metabolism to stomatal conductance. *Plant Sci.* **2015**, *241*, 32. [[CrossRef](#)]
29. Chen, G.; Zheng, Z.; Bai, M.; Li, Q. Chronic effects of microcystin-LR at environmental relevant concentrations on photosynthesis of *Typha angustifolia* Linn. *Ecotoxicology* **2020**, *29*, 514. [[CrossRef](#)]
30. Farquhar, G.D.; Caemmerer, S.V.; Berry, J.A. biochemical model of photosynthetic CO₂ assimilation in leaves of C₃ species. *Planta* **1980**, *149*, 78. [[CrossRef](#)]
31. Alencar, V.T.C.B.; Lobo, A.K.M.; Carvalho, F.E.L.; Silveira, J.A.G. High ammonium supply impairs photosynthetic efficiency in rice exposed to excess light. *Photosynth. Res.* **2019**, *140*, 321. [[CrossRef](#)] [[PubMed](#)]
32. Torralbo, F.; González-Moro, M.B.; Baroja-Fernández, E.; Aranjuelo, I.; González-Murua, C. Differential Regulation of Stomatal Conductance as a Strategy to Cope with Ammonium Fertilizer under Ambient versus Elevated CO₂. *Front. Plant Sci.* **2019**, *10*, 597. [[CrossRef](#)] [[PubMed](#)]
33. Li, H.; Wang, Y.; Xiao, J.; Xu, K. Reduced photosynthetic dark reaction triggered by ABA application increases intercellular CO₂ concentration, generates H₂O₂ and promotes closure of stomata in ginger leaves. *Environ. Exp. Bot.* **2015**, *113*, 11. [[CrossRef](#)]
34. Liu, M.; Liu, X.; Du, X.; Korpelainen, H.; Niinemets, Ü.; Li, C. Anatomical variation of mesophyll conductance due to salt stress in *Populus cathayana* females and males growing under different inorganic nitrogen sources. *Tree Physiol.* **2021**, *41*, 1462. [[CrossRef](#)] [[PubMed](#)]
35. Li, Y.; Ren, B.; Yang, X.; Xu, G.; Shen, Q.; Guo, S. Chloroplast Downsizing under Nitrate Nutrition Restrained Mesophyll Conductance and Photosynthesis in Rice (*Oryza sativa* L.) under Drought Conditions. *Plant Cell Physiol.* **2012**, *53*, 892. [[CrossRef](#)] [[PubMed](#)]
36. Onoda, Y.; Wright, I.J.; Evans, J.R.; Hikosaka, K.; Kitajima, K.; Niinemets, Ü.; Poorter, H.; Tosens, T.; Westoby, M. Physiological and structural tradeoffs underlying the leaf economics spectrum. *New Phytol.* **2017**, *214*, 1447. [[CrossRef](#)] [[PubMed](#)]
37. Flexas, J.; Clemente-Moreno, M.J.; Bota, J.; Brodribb, T.J.; Gago, J.; Mizokami, Y.; Nadal, M.; Perera-Castro, A.V.; Roig-Oliver, M.; Sugiura, D.; et al. Cell wall thickness and composition are involved in photosynthetic limitation. *J. Exp. Bot.* **2021**, *72*, 3971. [[CrossRef](#)]
38. Jian, S.; Liao, Q.; Song, H.; Liu, Q.; Lepo, J.E.; Guan, C.; Zhang, J.; Ismail, A.M.; Zhang, Z. NRT1.1-Related NH₄⁺ Toxicity Is Associated with a Disturbed Balance between NH₄⁺ Uptake and Assimilation. *Plant Physiol.* **2018**, *178*, 1473. [[CrossRef](#)]
39. Mao, L.Z.; Lu, H.F.; Wang, Q.; Cai, M.M. Comparative photosynthesis characteristics of *Calycanthus chinensis* and *Chimonanthus praecox*. *Photosynthetica* **2007**, *45*, 601. [[CrossRef](#)]
40. Brownlee, C. Stomatal Physiology: Cereal Successes. *Curr. Biol.* **2018**, *28*, R551. [[CrossRef](#)]
41. Andrés, Z.; Pérez-Hormaeche, J.; Leidi, E.O.; Schlücking, K.; Steinhorst, L.; McLachlan, D.H.; Schumacher, K.; Hetherington, A.M.; Kudla, J.; Cubero, B.; et al. Control of vacuolar dynamics and regulation of stomatal aperture by tonoplast potassium uptake. *Proc. Natl. Acad. Sci. USA* **2014**, *111*, E1806–E1814. [[CrossRef](#)] [[PubMed](#)]
42. Daszkowska-Golec, A.; Szarejko, I. Open or Close the Gate—Stomata Action under the Control of Phytohormones in Drought Stress Conditions. *Front. Plant Sci.* **2013**, *4*, 138. [[CrossRef](#)] [[PubMed](#)]
43. Gao, Y.; Li, Y.; Yang, X.; Li, H.; Shen, Q.; Guo, S. Ammonium nutrition increases water absorption in rice seedlings (*Oryza sativa* L.) under water stress. *Plant Soil* **2010**, *331*, 193. [[CrossRef](#)]
44. Kirscht, A.; Kaptan, S.S.; Bienert, G.P.; Chaumont, F.; Nissen, P.; de Groot, B.L.; Kjellbom, P.; Gourdon, P.; Johanson, U. Crystal Structure of an Ammonia-Permeable Aquaporin. *PLoS Biol.* **2016**, *14*, e1002411. [[CrossRef](#)] [[PubMed](#)]
45. Kapilan, R.; Vaziri, M.; Zwiazek, J.J. Regulation of aquaporins in plants under stress. *Biol. Res.* **2018**, *51*, 4. [[CrossRef](#)] [[PubMed](#)]
46. Li, Y.; Gao, Y.; Xu, X.; Shen, Q.; Guo, S. Light-saturated photosynthetic rate in high-nitrogen rice (*Oryza sativa* L.) leaves is related to chloroplastic CO₂ concentration. *J. Exp. Bot.* **2009**, *60*, 2351. [[CrossRef](#)] [[PubMed](#)]
47. Long, S.P. Gas exchange measurements, what can they tell us about the underlying limitations to photosynthesis? Procedures and sources of error. *J. Exp. Bot.* **2003**, *54*, 2393. [[CrossRef](#)]
48. Harley, P.C.; LFMG. Theoretical Considerations when Estimating the Mesophyll Conductance to CO₂ Flux by Analysis of the Response of Photosynthesis to CO₂. *Plant Physiol.* **1992**, *98*, 1429. [[CrossRef](#)]
49. Klughammer, C.; Schreiber, U. Complementary PS II quantum yields calculated from simple fluorescence parameters measured by PAM fluorometry and the Saturation Pulse method. *PAM Appl. Notes* **2008**, *1*, 27–35.
50. Nadal, M.; Brodribb, T.J.; Fernández Marín, B.; García Plazaola, J.I.; Arzac, M.I.; López Pozo, M.; Perera Castro, A.V.; Gulías, J.; Flexas, J.; Farrant, J.M. Differences in biochemical, gas exchange and hydraulic response to water stress in desiccation tolerant and sensitive fronds of the fern *Anemia cafferorum*. *N. Phytol.* **2021**, *231*, 1415. [[CrossRef](#)]
51. Zeng, Y.; Yu, J.; Cang, J.; Liu, L.; Mu, Y.; Wang, J.; Zhang, D. Detection of Sugar Accumulation and Expression Levels of Correlative Key Enzymes in Winter Wheat (*Triticum aestivum*) at Low Temperatures. *Biosci. Biotechnol. Biochem.* **2014**, *75*, 681. [[CrossRef](#)] [[PubMed](#)]
52. Greco, M.; Chiappetta, A.; Bruno, L.; Bitonti, M.B. In *Posidonia oceanica* cadmium induces changes in DNA methylation and chromatin patterning. *J. Exp. Bot.* **2012**, *63*, 695. [[CrossRef](#)] [[PubMed](#)]
53. Jiang, S.; Sun, J.; Tian, Z.; Hu, H.; Michel, E.J.S.; Gao, J.; Jiang, D.; Cao, W.; Dai, T. Root extension and nitrate transporter up-regulation induced by nitrogen deficiency improves nitrogen status and plant growth at the seedling stage of winter wheat (*Triticum aestivum* L.). *Environ. Exp. Bot.* **2017**, *141*, 28. [[CrossRef](#)]

54. Wu, S.; Sun, X.; Tan, Q.; Hu, C. Molybdenum improves water uptake via extensive root morphology, aquaporin expressions and increased ionic concentrations in wheat under drought stress. *Environ. Exp. Bot.* **2019**, *157*, 241. [[CrossRef](#)]
55. Yang, M.; He, J.; Sun, Z.; Li, Q.; Cai, J.; Zhou, Q.; Wollenweber, B.; Jiang, D.; Wang, X. Drought priming mechanisms in wheat elucidated by in-situ determination of dynamic stomatal behavior. *Front. Plant Sci.* **2023**, *14*, 1138494. [[CrossRef](#)]
56. Livak, K.J.; Schmittgen, T.D. Analysis of Relative Gene Expression Data Using Real-Time Quantitative PCR and the $2^{-\Delta\Delta CT}$ Method. *Methods* **2001**, *25*, 402. [[CrossRef](#)]

Disclaimer/Publisher's Note: The statements, opinions and data contained in all publications are solely those of the individual author(s) and contributor(s) and not of MDPI and/or the editor(s). MDPI and/or the editor(s) disclaim responsibility for any injury to people or property resulting from any ideas, methods, instructions or products referred to in the content.